

# Electronic Supporting Information For: Structural Variation in Ethylenediamine and -Diphosphine Adducts of (2,6-Me<sub>2</sub>C<sub>6</sub>H<sub>3</sub>S)<sub>2</sub>Pb: A Single Crystal X-ray Diffraction and <sup>207</sup>Pb Solid-State NMR Spectroscopy Study

2013, *Dalton Transactions*, DOI: 10.1039/c3dt33070b.

Aaron J. Rossini,<sup>a</sup> Alan W. Macgregor,<sup>a</sup> Gabriele Schatte,<sup>b</sup> Anita S. Smith,<sup>c</sup> Robert W. Schurko\*<sup>a</sup> and Glen G. Briand\*<sup>c</sup>

<sup>a</sup>Department of Chemistry & Biochemistry, University of Windsor, Windsor, Ontario, Canada, N9B 3P4

<sup>b</sup>Saskatchewan Structural Sciences Centre, University of Saskatchewan, Saskatoon, Saskatchewan Canada, S7N 5C9

<sup>c</sup>Department of Chemistry and Biochemistry, Mount Allison University, Sackville, New Brunswick, Canada, E4L 1G8

DOI:10.1039/c3dt33070b

## Table of Contents:

Table S1: CP/CPMG Experimental Parameters	S1
Table S2: WURST-QCPMG Experimental Parameters	S2
Table S3: Calculated <sup>31</sup> P NS Tensor Components for the Phosphorous Nuclei in <b>10</b>	S2
Table S4: Angles describing the orientation of MS tensor components	S3
Figure S1: <sup>207</sup> Pb VACP/MAS Spectrum of <b>12</b> and SIMPSON Simulations	S4
Figure S2: MAS <sup>31</sup> P{ <sup>1</sup> H} Solid-State NMR Spectrum of <b>11</b>	S5

**Table S1.** CP/CPMG Experimental Parameters

	<b>9</b>	<b>10</b>	<b>11</b>	<b>12</b>
Number of sub-spectra	19	22	23	20
Scans per sub-spectrum	192	120	120	128
Trans. Offset per piece (kHz)	20	24	24	20
Recycle delay (s)	20	30	30	45
Total Experiment Time (hours)	20	22	23	32
Number of Meiboom-Gill Loops	101	163	163	204
Real points per loop	80	50	50	40
Dwell ( $\mu$ s)	2.5	2.5	2.5	2.5
Spikelet Separation (kHz)	5	8	8	10
Acq. Length	8192	8192	8192	8192
pw90 ( $^1\text{H}$ ) ( $\mu$ s)	1.8	1.98	1.98	1.8
pw180 ( $^{207}\text{Pb}$ ) ( $\mu$ s)	3.6	3.5	3.5	3.6
Ring-down Delays ( $\tau_1 = \tau_2 = \tau_3 = \tau_4$ )	40	40	40	40
Contact time (s)	0.011	0.014	0.015	0.021
$\nu_1(^1\text{H})$ , decoupling (kHz)	53	53	53	53
$\nu_1(^1\text{H})$ , cross-polarization (kHz)	74	74	74	74
$\nu_1(^{207}\text{Pb})$ , cross-polarization (kHz)	43	43	43	43
Spectral width (kHz)	400	400	400	400

**Table S2.** WURST-QCPMG Experimental Parameters.

	<b>9</b>	<b>10</b>	<b>11</b>	<b>12</b>
Number of transients	1664	2400	808	759
Experimental time (hours)	41.6	60	20.2	19
WURST pulse offset (kHz)	1000	1000	1000	1000
Recycle delay (s)	90	90	90	90
Number of Meiboom-Gill Loops	100	100	200	200
Real points per loop	200	200	100	100
Spectral window of subspectra (kHz)	1000	1000	1000	1000
Dwell ( $\mu$ s)	1	1	1	1
Spikelet Separation (kHz)	10	5	10	10
Acq. Time (s)	0.02	0.02	0.02	0.02
WURST pulse length ( $\mu$ s)	50	50	50	50
WURST pulse rf field, $\nu_1(^{207}\text{Pb})$ (kHz)	7	7	7	7
Spectral width (kHz)	1000	1000	1000	1000

**Table S3.** Calculated  $^{31}\text{P}$  NS Tensor Components for the Phosphorous Nuclei in **10**.

	$\sigma_{11}$	$\sigma_{22}$	$\sigma_{33}$	$\sigma_{\text{iso}}$
site 1	161	313	387	287
site 2	172	312	396	293

The single crystal X-ray structure of **10** indicates that the two P nuclei magnetically equivalent. DFT calculations predict that there will be a 5 ppm difference between the isotropic chemical shifts of the two phosphorous nuclei ( $\Delta\sigma_{\text{iso}} = \Delta\delta_{\text{iso}}$ ). The shift difference predicted from the calculations most likely arises due to subtle differences in the proton coordinates in the molecular fragment used for calculations.

**Table S4.** Angles describing the orientation of MS tensor components with respect to key structural and symmetry elements.

<b>Compound 12</b>			
$\sigma_{33}$ -Pb-S (1)	119.3°		
$\sigma_{33}$ -Pb-S (2)	133.4°		
$\sigma_{33}$ -Pb-S (3)	116.2°		
<b>Compound 11</b>			
$\sigma_{33}$ -Pb-S (1)	141.0°		
$\sigma_{33}$ -Pb-S (2)	122.0°		
$\sigma_{33}$ -Pb-P	98.4°		
<b>Compound 9 (Site 1, PbS<sub>2</sub>N<sub>2</sub>)</b>		<b>(Site 2, PbS<sub>3</sub>)</b>	
$\sigma_{33}$ -Pb-S (1)	163.5°	$\sigma_{33}$ -Pb-S (1)	113.9°
$\sigma_{33}$ -Pb-S (2)	94.1°	$\sigma_{33}$ -Pb-S (2)	138.0°
$\sigma_{33}$ -Pb-N (1)	103.4°	$\sigma_{33}$ -Pb-S (3)	108.9°
$\sigma_{33}$ -Pb-N (2)	81.5°		
<b>Compound 10 (Site 1, PbP<sub>2</sub>S<sub>2</sub>)</b>		<b>(Site 2, PbS<sub>3</sub>)</b>	
$\sigma_{33}$ -Pb-S (1)	10.7°	$\sigma_{33}$ -Pb-S (1)	142.4°
$\sigma_{33}$ -Pb-S (2)	163.5°	$\sigma_{33}$ -Pb-S (2)	121.7°
$\sigma_{33}$ -Pb-P (1)	88.3°	$\sigma_{33}$ -Pb-S (3)	98.4°
$\sigma_{33}$ -Pb-P (2)	86.8°		

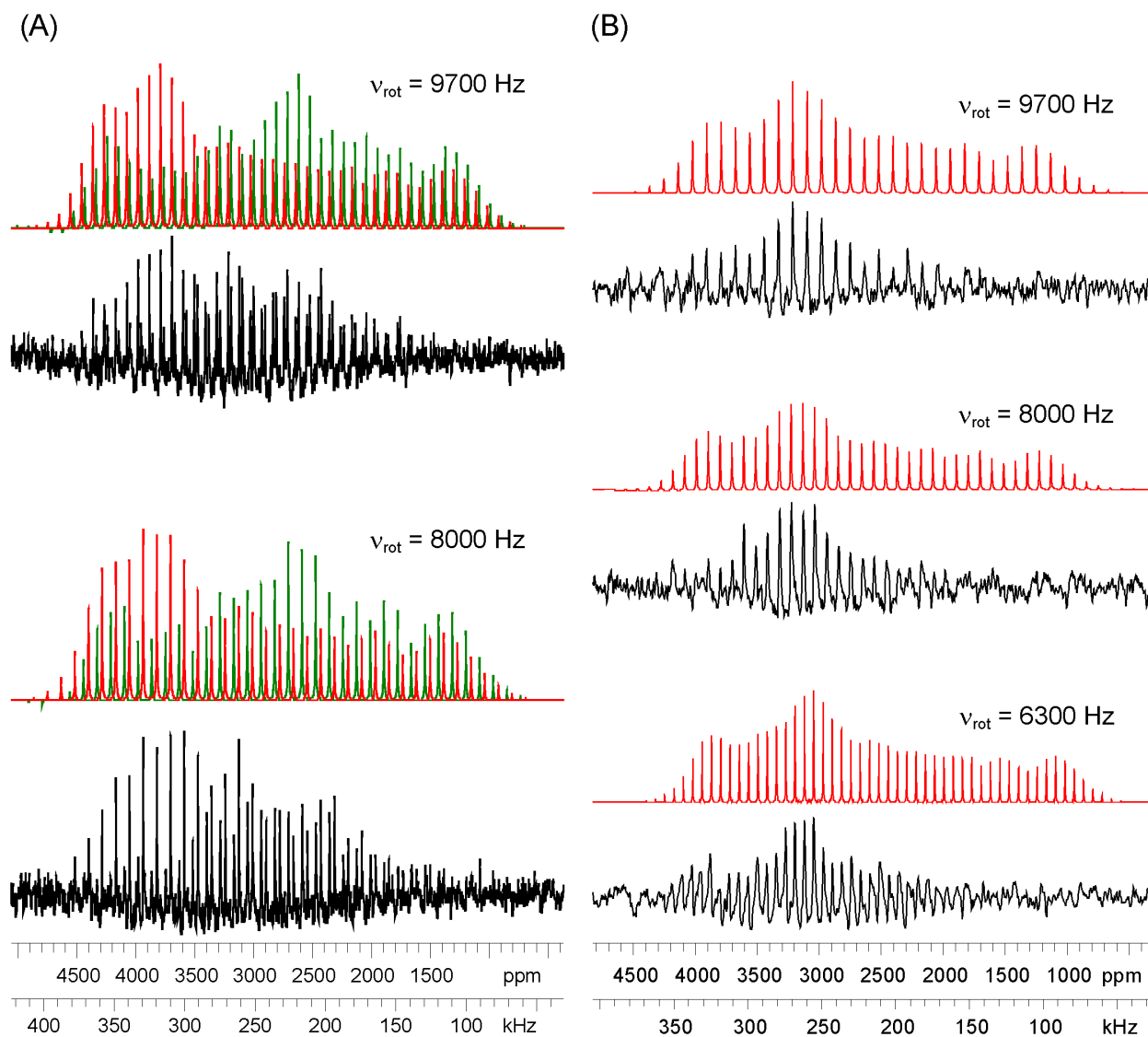


**Figure S1.** SIMPSON simulations (top colored traces) and experimental  $^{207}\text{Pb}$  CP/MAS spectra (bottom black traces) of **9** (A) and **12** (B). The sample spinning rates are indicated next to the simulated spectra. For **9**, simulations of the site 1 ( $\text{PbS}_3$ , red trace) and site 2 ( $\text{PbS}_2\text{N}_2$ , green trace) were performed separately. All simulations were performed with ideal rf pulses ( $I_X$  starting operator).

11

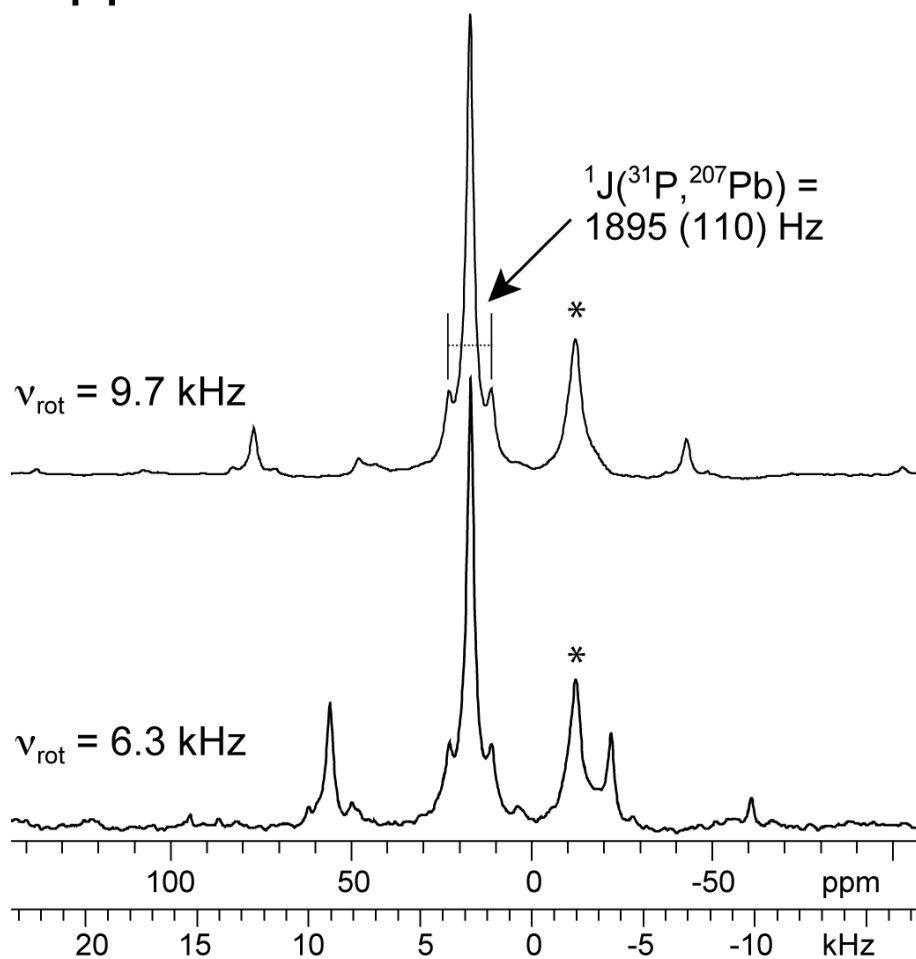


**Figure S2.**  $^{31}\text{P}\{^1\text{H}\}$  MAS NMR spectra of  $[(2,6\text{-Me}_2\text{C}_6\text{H}_3\text{S})_2\text{Pb}]_2(\text{dppe})$  (**11**). \* denotes impurity. The spectra were referenced to 85%  $\text{H}_3\text{PO}_4$  ( $\delta_{\text{iso}} = 0.0 \text{ ppm}$ )